Published in final edited form as:
Cell Metab. 2012 September 5; 16(3): 311–321. doi:10.1016/j.cmet.2012.08.004.

Maintenance of metabolic homeostasis by Sestrin 2 and 3

Jun Hee Lee[1,6,*,12], **Andrei V. Budanov**[1,8,12], **Saswata Talukdar**[2], **Eek Joong Park**[1], **Hae Li Park**[6], **Hwan-Woo Park**[6], **Gautam Bandyopadhyay**[2], **Ning Li**[1], **Mariam Aghajan**[1], **Insook Jang**[6], **Amber M. Wolfe**[7], **Guy A. Perkins**[3], **Mark H. Ellisman**[3], **Ethan Bier**[4], **Miriam Scadeng**[5], **Marc Foretz**[9,10,11], **Benoit Viollet**[9,10,11], **Jerrold Olefsky**[2], and **Michael Karin**[1,*]

[1]Laboratory of Gene Regulation and Signal Transduction, Departments of Pharmacology and Pathology, University of California, San Diego, San Diego, CA 92093, USA.

[2]Department of Medicine, Division of Endocrinology and Metabolism, University of California, San Diego, San Diego, CA 92093, USA.

[3]National Center for Microscopy and Imaging Research, and Department of Neurosciences, University of California, San Diego, San Diego, CA 92093, USA.

[4]Section of Cell and Developmental Biology, University of California, San Diego, San Diego, CA 92093, USA.

[5]Department of Radiology, University of California, San Diego, San Diego, CA 92093, USA.

[6]Department of Molecular and Integrative Physiology, University of Michigan, Ann Arbor, MI 48109, USA.

[7]Unit for Laboratory Animal Medicine, University of Michigan, Ann Arbor, MI 48109, USA.

[8]Department of Neurosurgery, Virginia Commonwealth University, Richmond, VA 23298, USA.

[9]Inserm U1016, Institut Cochin, Paris, France.

[10]Cnrs, UMR8104, Paris, France.

[11]Université Paris Descartes, Sorbonne Paris cité, Paris, France.

Summary

Chronic activation of mammalian target of rapamycin complex 1 (mTORC1) and p70 S6 kinase (S6K) in response to hypernutrition contributes to obesity-associated metabolic pathologies including hepatosteatosis and insulin resistance. Sestrins are stress-inducible proteins that activate AMP-activated protein kinase (AMPK) and suppress mTORC1-S6K activity, but their role in mammalian physiology and metabolism has not been investigated. We show that Sestrin2, encoded by the *Sesn2* locus whose expression is induced upon hypernutrition, maintains metabolic homeostasis in liver of obese mice. *Sesn2* ablation exacerbates obesity-induced mTORC1-S6K activation, glucose intolerance, insulin resistance and hepatosteatosis, all of which are reversed by AMPK activation. Furthermore, concomitant ablation of *Sesn2* and *Sesn3* provokes hepatic mTORC1-S6K activation and insulin resistance even in the absence of nutritional overload and obesity. These results demonstrate an important homeostatic function for the stress-inducible Sestrin protein family in the control of mammalian lipid and glucose metabolism.

[*]Correspondence: leeju@umich.edu; karinoffice@ucsd.edu, **Contact**: Michael Karin, karinoffice@ucsd.edu, Phone: 858-534-1361, Fax: 858-534-8158.

[12]These authors contributed equally to this work.

Introduction

Over-nutrition and sedentary lifestyle are major contributors to the obesity epidemic, which affects one third of U.S. adults and up to 1 billion people worldwide (Haslam and James, 2005). As a consequence, obesity-associated diseases, such as diabetes, cardiovascular disease and non-alcoholic fatty liver disease, have become a major public health problem. Obesity also increases cancer risk, with the most pronounced effect exerted on hepatocellular carcinoma, the prevalent type of liver cancer (Calle et al., 2003). In obese individuals, excessive nutrients are stored as fat in liver and adipose tissues. Accumulation of fat droplets in the liver, a condition known as hepatosteatosis, can eventually lead to chronic liver inflammation (steatohepatitis), liver damage, diabetes and liver cancer (Angulo, 2002).

mTORC1 is an evolutionarily conserved protein kinase that senses nutrient availability and controls cellular metabolism. Nutritional abundance can lead to chronic mTORC1 activation, thereby enhancing protein and lipid biosynthesis and inhibiting autophagic catabolism (Um et al., 2006; Zoncu et al., 2011). Through its substrate S6K, mTORC1 causes inhibitory serine phosphorylation of insulin receptor substrates (IRS), thereby contributing to insulin resistance and subsequent attenuation of insulin-induced AKT activity (Bae et al., 2012; Um et al., 2006). Chronic inhibition of autophagy attenuates clearance of liver lipid droplets (LDs), thereby contributing to hepatosteatosis (Singh et al., 2009). Thus chronic mTORC1 activation upon persistent hypernutrition and lack of exercise can give rise to insulin resistance and lipid accumulation and eventually drive the pathogenesis of type II diabetes and steatohepatitis (Zoncu et al., 2011). Downregulation of autophagy can also lead to accumulation of damaged mitochondria and reactive oxygen species (ROS), giving rise to tissue degeneration and increased cancer risk (Mizushima and Komatsu, 2011).

To avoid the pathogenic consequences of chronic mTORC1 activation, several negative feedback loops have evolved. Using *Drosophila* as a model organism, we found that chronic dTORC1 activation results in transcriptional activation of the *dSesn* locus that encodes for *Drosophila* Sestrin (Lee et al., 2010). dSestrin belongs to a highly conserved family of stress-inducible proteins, which in mammals includes Sestrin1, Sestrin2 and Sestrin3 (Budanov et al., 2010). Once induced, the Sestrins potentiate AMPK activation and thereby enhance phosphorylation of tuberous sclerosis complex 2 (TSC2), which in turn attenuates mTORC1 activation and stimulates autophagy (Budanov and Karin, 2008; Maiuri et al., 2009). The AMPK-activating and mTORC1-suppressing activities of the Sestrins are conserved between insects and mammals (Lee et al., 2010), but the physiological functions of the mammalian Sestrins remain to be identified. Loss of dSestrin results in diverse age- and obesity-associated pathologies, such as fat accumulation and cardiac dysfunction, all of which are precipitated by activation of dTORC1 (Lee et al., 2010). Given the biochemical similarities between *Drosophila* and mammalian Sestrins, we postulated that mammalian Sestrins may also have important homeostatic functions during conditions that cause excessive mTORC1 activation. Here we describe such a function for Sestrin2 and Sestrin3 in control of liver insulin resistance and lipid accumulation before and during obesity.

Results

Sestrin2 deficiency enhances obesity-induced insulin resistance and diabetic progression

Sesn2$^{-/-}$ mice are fully viable and do not display any gross developmental abnormalities (Budanov and Karin, 2008). Body weight as well as glucose homeostasis and insulin responsiveness evaluated by glucose tolerance (GTT) and insulin tolerance (ITT) tests, respectively, were not significantly different between control (Con; either *Sesn2*$^{+/+}$ or

Sesn2$^{+/-}$) and *Sesn2*$^{-/-}$ mice when maintained on normal chow (low fat diet; LFD) (Figures S1A–S1C).

Expression of *Sesn2* mRNA in liver was elevated in mice kept on high fat diet (HFD), in which 60% of the calories were fat-derived, while *Sesn1* and *Sesn3* mRNAs were not affected (Figure S1D). As a result, Sestrin2 protein accumulated in liver of obese mice kept on HFD (Figures S1E–S1G). Loss of Sestrin2 had marginal effects on liver Sestrin1 and Sestrin3 expression in obese mice (Figures S1G–S1I). Obesity-induced accumulation of Sestrin2 was also observed in skeletal muscle, but not in adipose tissue (Figure S1G). Since Sestrin2 is an obesity-inducible protein, we examined whether Sestrin2 deficiency affected weight gain and glucose homeostasis in mice kept on HFD. As observed in LFD animals, *Sesn2*$^{-/-}$ mice on HFD did not differ in weight gain (Figure S1J) or food consumption (Figure S1K) from Con mice. Nonetheless, the Sestrin2 deficiency had a pronounced effect on glucose homeostasis and insulin responsiveness in mice kept on HFD. GTT and ITT indicated a significantly higher degree of glucose intolerance (Figures 1A and 1B) and insulin resistance (Figures 1C and 1D) in *Sesn2*$^{-/-}$mice relative to Con counterparts after 3 months of HFD. However, there was no significant defect in insulin secretion during GTT (Figure S1L).

To examine the effect of Sestrin2 ablation in a genetic model of obesity, we intercrossed *Sesn2*$^{-/-}$ and *Lep*$^{ob/ob}$ mice. As seen with diet-induced obesity, *Lep*$^{ob/ob}$/*Sesn2*$^{-/-}$ mice were more glucose intolerant (Figures 1E and 1F) and insulin resistant (Figures 1G and 1H) than *Lep*$^{ob/ob}$/*Sesn2*$^{+/-}$ mice. However, the Sestrin2 deficiency had no effect on body weight (Figure S1M) or food consumption (Figure S1N) of *Lep*$^{ob/ob}$ mice. Magnetic resonance imaging (MRI) of *Lep*$^{ob/ob}$/*Sesn2*$^{+/-}$ and *Lep*$^{ob/ob}$/*Sesn2*$^{-/-}$ mice reaffirmed their similar body mass and visceral and subcutaneous fat pad volumes (Figures S1O and S1P). Nonetheless, at 4 months of age, *Lep*$^{ob/ob}$/*Sesn2*$^{-/-}$ mice became severely diabetic, exhibiting much higher fasting blood glucose than *Lep*$^{ob/ob}$/*Sesn2*$^{+/-}$ mice (Figure 1I), and started excreting large amounts of glucose in their urine (Figure 1J).

Sesn2$^{-/-}$ mice display defective insulin responsiveness in liver and adipose tissue

To better understand the basis for defective glucose homeostasis and insulin responsiveness in obese *Sesn2*$^{-/-}$ mice, we performed hyperinsulinemic-euglycemic clamp studies (Figures S2A–S2C). Upon insulin infusion, *Sesn2*$^{-/-}$ mice kept on HFD exhibited a significantly lower glucose infusion rate (GIR), confirming the presence of whole body insulin resistance (Figure 2A). However, *Sesn2*$^{-/-}$ mice did not differ from Con mice with respect to insulin-stimulated glucose disposal rate (IS-GDR), indicative of muscle insulin responsiveness (Figure 2B). However, suppression of hepatic glucose production (HGP) during the hyperinsulinemic-euglycemic clamp was substantially reduced in *Sesn2*$^{-/-}$ mice (Figure 2C). Consequently, more than 80% of the effect of Sestrin2 loss on GIR reduction was attributable to the decreased HGP suppression while the contribution of insulin-induced glucose uptake changes in peripheral tissues was minimal and not statistically significant. These indications suggest that defective glucose homeostasis in *Sesn2*$^{-/-}$ mice is largely due to decreased hepatic insulin sensitivity.

We also examined insulin responsiveness in adipose tissue. Suppression of serum free fatty acids (FFA) during the hyperinsulinemic-euglycemic clamp studies provides an indirect assessment of adipocyte insulin sensitivity. Although FFA suppression was modestly reduced in *Sesn2*$^{-/-}$ mice, the difference did not reach significance (Figures S2D and S2E). To more directly measure adipose tissue insulin responsiveness, we measured insulin-induced glucose uptake by primary adipocytes isolated from Con and *Sesn2*$^{-/-}$ mice kept on HFD. Whereas glucose uptake in Con adipocytes was stimulated 2.5-fold by insulin,

Sesn2$^{-/-}$ adipocytes exhibited markedly reduced insulin responsiveness (Figures S2F and S2G), suggesting that Sestrin2 controls insulin sensitivity also in adipose tissue.

Compromised insulin-stimulated PI3K-AKT signaling in liver of *Sesn2*$^{-/-}$ mice

AKT is an important effector of insulin signaling in liver and adipose tissue, mainly controlling glucose and lipid metabolism (Manning and Cantley, 2007). To examine whether Sestrins, which control AMPK and mTORC1 activity (Budanov and Karin, 2008; Lee et al., 2010), also modulate insulin-induced AKT activation, we examined AKT phosphorylation in livers of Con and *Sesn2*$^{-/-}$ mice kept on HFD before and after insulin administration. In Con liver, insulin treatment induced AKT phosphorylation at Thr308 and Ser473, the two sites responsible for AKT activation. However in *Sesn2*$^{-/-}$ livers, insulin-induced AKT phosphorylation at both sites was substantially reduced (Figures 2D and 2E). AKT activation results in inhibitory phosphorylation of forkhead box O (FoxO)-family transcription factors including FoxO1, leading to reduced expression of genes that encode gluconeogenic enzymes such as phosphoenolpyruvate carboxykinase (PEPCK). In *Sesn2*$^{-/-}$ mice, AKT-dependent FoxO1 phosphorylation was decreased (Figure 2D) and *Pepck* mRNA amounts were elevated relative to Con mice (Figure S2H). These results indicate that Sestrin2 is required for maintenance of insulin-induced AKT activation and its sequelae during obesity.

Consistent with the hyperinsulinemic-euglycemic clamp studies showing that muscle insulin responsiveness is not affected by loss of Sestrin2 (Figure 2B), insulin-induced AKT phosphorylation was largely similar between Con and *Sesn2*$^{-/-}$ muscle tissue (Figures S2I and S2J). In *Sesn2*$^{-/-}$ adipose tissue, insulin-induced AKT phosphorylation was slightly reduced relative to Con (Figures S2K and S2L).

To find out the mechanism through which insulin-induced AKT signaling is downregulated in *Sesn2*$^{-/-}$ mouse liver, we analyzed activities of signaling components that act upstream of AKT. We found that insulin-stimulated phosphoinositide 3-kinase (PI3K) activity in liver of *Sesn2*$^{-/-}$ mice was lower than that of Con liver (Figures 2F and 2G). Insulin-induced tyrosine phosphorylation of IRS-1 was also reduced in *Sesn2*$^{-/-}$ liver compared to Con liver (Figure 2H), suggesting that insulin resistance in *Sesn2*$^{-/-}$ liver occurs upstream or at the level of IRS-1. Interestingly, Ser632 phosphorylation of IRS-1 (corresponding to Ser636 in human IRS-1), which opposes IRS-1 tyrosine phosphorylation (Boura-Halfon and Zick, 2009), was significantly higher in *Sesn2*$^{-/-}$ liver both before and especially after insulin treatment (Figures 2H and 2I).

Sestrin2 attenuates chronic mTORC1 activation during obesity

As Ser632 phosphorylation of IRS-1 is mediated through S6K (Um et al., 2004), a mTORC1 target, we postulated that Sestrin2 regulates insulin signaling sensitivity through the AMPK-mTORC1-S6K axis. Therefore, we examined whether mTORC1-S6K signaling is affected by Sestrin2 loss. As previously reported (Um et al., 2004), mTORC1-dependent activatory S6K phosphorylation at both Thr389 and Ser411 (Ali and Sabatini, 2005) was modestly elevated in livers of Con mice kept on HFD compared to LFD-kept mice (Figures 3A and 3B). However, in liver of *Sesn2*$^{-/-}$ mice kept on HFD, the increase in S6K phosphorylation compared to LFD-fed *Sesn2*$^{-/-}$ and even HFD-kept Con liver was much larger (Figures 3A and 3B), suggesting that Sestrin2 attenuates chronic liver mTORC1-S6K signaling upon nutritional overload. The chronic upregulation of S6K was found in both basal and insulin-stimulated liver tissues of *Sesn2*$^{-/-}$ mice kept on HFD (Figure 3C). However, there were no significant changes in S6K phosphorylation between livers of Con and *Sesn2*$^{-/-}$ mice kept on LFD (Figures 3A and 3B), and this is consistent with the low expression of Sestrin2 in

lean mice (Figures S1D–S1G) and the absence of metabolic abnormalities in *Sesn2*$^{-/-}$ mice kept on LFD (Figures S1A–S1C).

We previously showed that Sestrins negatively regulate the mTORC1-S6K axis by potentiating AMPK activation (Budanov and Karin, 2008; Lee et al., 2010). Livers of *Sesn2*$^{-/-}$mice kept on HFD exhibited lower activatory AMPK phosphorylation (Figures 3C and 3D) and decreased AMPK catalytic activity (Figures 3E and S3A). Livers of *Sesn2*$^{-/-}$/*Lep*$^{ob/ob}$ mice also exhibited lower AMPK activity than *Sesn2*$^{+/-}$/*Lep*$^{ob/ob}$ livers (Figures 3F and S3B). The decrease in AMPK activity was particularly striking because total AMPK amounts increased upon Sestrin2 loss in both HFD- and *Lep*^{ob}-induced obese mice (Figure 3C, S3A and S3B), suggesting that low AMPK and high mTORC1 activity in obese Sestrin2-deficient livers led to a compensatory increase in AMPK protein expression. AMPK-dependent phosphorylation of acetyl-CoA carboxylase (ACC) at Ser79 was modestly reduced in Sestrin2-deficient obese livers (Figure S3C). Conversely, autophosphorylation of mTOR at Ser2481, an indicator of mTORC1 catalytic activity (Soliman et al., 2010), was higher in *Sesn2*$^{-/-}$/*Lep*$^{ob/ob}$ livers than in *Sesn2*$^{+/-}$/*Lep*$^{ob/ob}$ livers (Figure S3D). Correspondingly, S6K catalytic activity, which is directly stimulated by mTORC1, was elevated in *Sesn2*$^{-/-}$/*Lep*$^{ob/ob}$ livers relative to *Sesn2*$^{+/-}$/*Lep*$^{ob/ob}$ livers (Figures 3G and S3E). S6K-mediated inhibitory phosphorylation of IRS-1 at Ser632 and Ser635 (Um et al., 2004) was also substantially elevated in *Sesn2*$^{-/-}$ obese livers (Figures S3F–S3I). Thus, Sestrin2 is a positive regulator of AMPK activation in the obese liver that is required for keeping mTORC1 activity suppressed.

Sestrin2 loss modestly decreased liver AMPK activity in lean mice (Figure S3J). However, mTORC1 activity, monitored by its target S6K, was similar between Con and *Sesn2*$^{-/-}$mice (Figure S3K), and insulin-induced AKT activation in liver (Figure S3L) and in adipose tissue (Figure S3M) was also comparable between lean Con and *Sesn2*$^{-/-}$ mice. These results suggest that, in the absence of nutritional overload or obesity, conditions that increase Sestrin2 expression, lower AMPK activity caused by loss of basal Sestrin2 expression is insufficient to cause mTORC1 hyperactivation and insulin resistance.

AMPK activation restored insulin sensitivity in *Sesn2*$^{-/-}$ mice

If Sestrin2's protective effect against obesity-induced insulin resistance is exerted through modulation of AMPK and mTORC1 activities, restoration of AMPK activity or suppression of chronic mTORC1 should restore insulin signaling to obese *Sesn2*$^{-/-}$ mice. Therefore, we attempted to suppress chronic mTORC1 activity in *Sesn2*$^{-/-}$ mice using rapamycin. Although rapamycin administration suppressed mTORC1-S6K signaling in *Sesn2*$^{-/-}$ liver, it failed to restore blood glucose homeostasis in obese *Sesn2*$^{-/-}$ mice (data not shown). However, it was recently shown that long-term rapamycin administration to mice can suppress mTORC2, which is critical for AKT activation and insulin responsiveness (Lamming et al., 2012). Therefore, we used AICA-ribonucleotide (AICAR), which can effectively suppress hepatic mTORC1 activity through AMPK activation without affecting mTORC2 (Reiter et al., 2005). Although AICAR administration caused only a slight reduction in basal hyperglycemia and glucose intolerance (Figures S4A and S4B), it significantly restored insulin responsiveness of HFD-kept *Sesn2*$^{-/-}$mice (Figure 4A), suggesting that AICAR-mediated AMPK reactivation can correct the insulin resistance phenotype caused by Sestrin2 loss. Indeed in the liver, AICAR also restored AMPK activity and suppressed mTORC1-S6K activity (Figure 4B), and restored insulin-induced AKT activation (Figures 4C and S4C). Furthermore, liver-specific transduction of adenoviruses expressing constitutively-active AMPK (Ad-AMPK^{CA}) (Figure S4D) was sufficient to suppress insulin resistance in HFD-kept *Sesn2*$^{-/-}$ mice (Figures 4D and 4E). These data strongly suggest that Sestrin2 maintains hepatic insulin sensitivity by promoting AMPK activation in liver.

Sestrin2 loss aggravates hepatosteatosis caused by dietary or genetic obesity

Decreased AMPK and increased mTORC1 activities are associated with fat accumulation (Kahn et al., 2005; Laplante and Sabatini, 2009), and Sestrin is important for prevention of fat droplet accumulation in the *Drosophila* fat body (Lee et al., 2010), an equivalent of the mammalian liver (Sondergaard, 1993). Indeed, Sestrin2 deficiency aggravated hepatosteatosis caused by dietary or genetic obesity. In lean mice, liver triglycerides were only slightly elevated in $Sesn2^{-/-}$ livers compared to Con livers (Figure 5A). However, when mice were kept on HFD, liver triglycerides were substantially higher in $Sesn2^{-/-}$ livers than in Con livers (Figure 5A). $Sesn2^{-/-}$ livers also exhibited increased LD accumulation revealed by oil red O staining (Figure 5B). Transmission electron microscopy (EM) showed that the size of LDs was increased upon loss of Sestrin2 under HFD conditions (Figures 5C and 5D). Livers of $Sesn2^{-/-}/Lep^{ob/ob}$ mice also contained higher amounts of triglycerides than $Sesn2^{+/-}/Lep^{ob/ob}$ livers (Figure 5A).

Diminished autophagy, as a result from Sestrin2 loss, AMPK inhibition and mTORC1 activation (Chan, 2009; Egan et al., 2011; Maiuri et al., 2009), can contribute to accumulation of LDs in liver (Singh et al., 2009). EM analysis revealed that in livers of Con mice on HFD, many LDs were associated with vesicles surrounded by double membranes (Figures 5C and S5A). Such structures were barely detectable on the much larger LDs in $Sesn2^{-/-}$ hepatocytes of mice on HFD (Figures 5C, S5B and S5C). Based on previous reports these structures most likely represent autophagic vesicles (AV) engaged in LD digestion (Singh et al., 2009). Consistent with this, immunofluorescence imaging of LD and the AV marker LC3 showed a considerable colocalization of both structures in Con liver but not in $Sesn2^{-/-}$ liver from mice kept on HFD (Figure S5D). Although the association of LD with AV was dramatically decreased in livers of $Sesn2^{-/-}$ HFD-kept mice, the difference between LFD-kept Con and $Sesn2^{-/-}$mice was much less prominent (Figure S5C).

Lower AMPK activity in liver could also result in decreased mitochondrial biogenesis and reduced β-oxidation of fatty acids, which contributes to lipid accumulation (Kahn et al., 2005). Indeed, fewer mitochondria were observed in liver EM images of HFD-kept $Sesn2^{-/-}$ mice than Con mice (Figure 5E), and reduced mitochondrial content was confirmed by quantitative PCR of mitochondrial DNA (Figures S5E and S5F). In addition, Sestrin2 deficiency resulted in reduced expression of two mitochondrial biogenesis marker genes, *Tfam* and *Nrf1* (Figures 5F and S5G). Consistent with these results, β-oxidation of palmitic acid by liver homogenates was also reduced upon Sestrin2 deficiency in $Lep^{ob/ob}$ mice (Figure 5G) and hepatic AMPK restoration through AICAR or Ad-$AMPK^{CA}$ suppressed liver triglyceride accumulation (Figures S4E and S4F).

Chronic AMPK downregulation and mTORC1 activation can promote processing and nuclear translocation of the lipogenic transcription factor SREBP (Li et al., 2011; Porstmann et al., 2008). Correspondingly, $Sesn2^{-/-}/Lep^{ob/ob}$ livers contained more processed SREBP than $Sesn2^{+/-}/Lep^{ob/ob}$ livers, and the processed SREBP was translocated into the nucleus (Figures S5H–S5J). However, Sestrin2 loss caused only a modest increase in SREBP-dependent gene expression and the effects varied between mice with dietary and genetic obesity (Figures S5K and S5L). The lipogenic activity of the $Sesn2^{-/-}/Lep^{ob/ob}$ liver was also not significantly increased when compared to control $Sesn2^{+/-}/Lep^{ob/ob}$ livers (Figure S5M). These results suggest that the decreased lipid β-oxidation in Sestrin2-deficient livers due to reduced autophagy and/or mitochondrial biogenesis, rather than increased lipogenesis, is the main cause of hepatosteatosis.

Concomitant loss of Sestrin2 and 3 causes spontaneous insulin resistance

Unlike *dSesn*-null flies that show spontaneous metabolic abnormalities (Lee et al., 2010), lean *Sesn2*$^{-/-}$ mice do not develop spontaneous hepatosteatosis or glucose homeostasis defects. This may be due to the existence of multiple mammalian *Sesn* homologues that compensate for Sestrin2 loss. To examine this possibility, we generated *Sesn3*$^{-/-}$ mice from a *Sesn3*-targeted ES cell line (Friedel et al., 2007). *Sesn3*$^{-/-}$ mice were intercrossed with *Sesn2*$^{-/-}$ mice to generate *Sesn2*$^{-/-}$/*Sesn3*$^{-/-}$ (DKO) mice (Figure S6A). Although the DKO mice did not exhibit spontaneous obesity (Figure S6B) or hepatosteatosis (Figure S6C) on LFD, they exhibited higher S6K phosphorylation (Figures 6A, 6B, S6D–S6G) and lower insulin-induced AKT phosphorylation than Con mice (Figures 6C, 6D, S6H–S6K) in both liver and muscle, effects that were not observed in LFD-fed *Sesn2*$^{-/-}$ mice (Figures 3A and S3L). Correspondingly, DKO mice on LFD exhibited insulin resistance and glucose intolerance (Figures 6E, 6F and S6L), relative to Con mice. These results suggest that both Sestrin2 and Sestrin3 are required for proper blood glucose homeostasis under normal conditions.

Sestrins promote AKT phosphorylation through inhibition of mTORC1

Finally, using cultured cells, we determined if Sestrins can regulate insulin-PI3K-AKT signaling in a cell autonomous manner. In *Sesn2*$^{-/-}$ mouse embryonic fibroblasts (MEFs), both basal (Figure 7A) and insulin-stimulated (Figure 7B) AKT phosphorylation at Thr308 and Ser473 was reduced relative to *Sesn2*$^{+/-}$ MEFs. When overexpressed in MCF7, H1299 and HepG2 cells, Sestrin2 increased AKT phosphorylation even without insulin stimulation (Figures 7C, S7A and S7B). The same effect was exhibited by Sestrin1, Sestrin3 and dSestrin (Figures S7A and S7C), indicating that the AKT regulatory function is conserved throughout the Sestrin family. Phosphorylation of AKT downstream targets including FoxO3A, GSK3 and TSC2, as well as the lipid kinase activity of PI3K, was also increased upon Sestrin2 expression (Figures S7A, S7D and S7E). Although mTORC1-dependent S6K phosphorylation was decreased by Sestrin2 as previously reported (Budanov and Karin, 2008), phosphorylation of ERK and RSK was unaffected (Figure S7D), indicating the specificity of the Sestrin2 effect on the PI3K-AKT signaling pathway.

Given that Sestrin2 can function as a redox regulator (Budanov et al., 2004), it may potentiate insulin-induced AKT activation by preventing ROS accumulation (Cao et al., 2009). However, a redox-deficient Sestrin2 mutant (Sestrin2^{CS}) was fully capable of inducing AKT phosphorylation when overexpressed (Figure S7F). Expression of peroxiredoxin 1 (Prx1), which inhibits ROS accumulation through the same pathway as Sestrin2 (Budanov et al., 2004), had no effect on AKT phosphorylation (Figure S7F). These results indicate that Sestrin2 redox activity is dispensable for the effects on AKT activation.

We examined whether AMPK activation and suppression of mTORC1 activity are responsible for Sestrin2-induced activation of AKT. Indeed, activation of AKT by Sestrin2 was not observed in *Tsc2*$^{-/-}$ (Figure 7D) and *Ampk*^{null} (*Ampkα1*$^{-/-}$/*Ampkα2*$^{-/-}$; Figure 7E) MEFs, in both of which mTORC1 activity is no longer affected by Sestrins (Budanov and Karin, 2008). Silencing of TSC2 (Figure S7G) or AMPKα1 (Figure S7H) with shRNA lentiviruses also compromised activation of AKT by Sestrin2 in the MCF7 tet-OFF cells. On the other hand, inhibition of mTORC1 through short-term treatment of rapamycin enhanced AKT phosphorylation to the same extent as Sestrin2 expression (Figure S7I), while Sestrin2 was unable to promote AKT activation in the absence of Rictor, a critical component of mTORC2 Figures S7J and S7K). These results indicate that Sestrin2 controls AKT phosphorylation through the AMPK-mTORC1/2 signaling axis in multiple cell types.

As observed in mammalian cells, both wild-type and redox-inactive dSestrin induced AKT phosphorylation when expressed in the dorsal part of *Drosophila* wing discs (Figures 7F–7H). Activation of AKT by Sestrin in *Drosophila* was mediated through the AMPK-dTORC1 axis, since silencing of AMPK (Figure 7I) or expression of Rheb (Figure 7J) or $S6K^{CA}$ (Figure 7K) suppressed induction of AKT phosphorylation by dSestrin. In addition, $dSesn^{-/-}$ adult flies showed elevated blood trehalose concentration (Figure S7L), suggesting that Sestrin-dependent control of AKT signaling and blood sugar homeostasis is evolutionarily conserved.

Discussion

The AMPK-mTORC1 axis is a well-established and conserved central regulator of cellular metabolism (Kahn et al., 2005; Zoncu et al., 2011). In cultured mammalian cells subjected to genotoxic stress and in *Drosophila*, the AMPK-mTORC1 axis output is modulated by expression of Sestrin proteins (Budanov and Karin, 2008; Chen et al., 2010; Lee et al., 2010). However, given the existence of three mammalian *Sesn* genes, whose protein products exhibit conserved biochemical functions (Budanov et al., 2004; Budanov and Karin, 2008), a physiological role for Sestrins in metabolic regulation could previously be observed only in *Drosophila* (Lee et al., 2010). Early experiments suggested that the Sestrins regulate information flow through the AMPK-mTORC1 axis during genotoxic or oxidative stress, which result in their transcriptional upregulation via p53 (Budanov and Karin, 2008) and FoxO3A (Nogueira et al., 2008). The current results, however, indicate that the mammalian Sestrins also have important physiological functions that are not limited to acute stress conditions. Here we show that Sestrin2 and 3 have physiologically relevant homeostatic functions both before and during obesity in the control of insulin signaling and blood glucose metabolism. This function is probably exerted through Sestrins' ability to promote AMPK activation and suppress mTORC1-S6K signaling (Budanov and Karin, 2008).

The glucose homeostasis disorder observed in obese $Sesn2^{-/-}$ mice is mainly due to hepatic insulin resistance, which is reversible by AMPK reactivation through AICAR and adenovirus-mediated transduction. AMPK reactivation also strongly suppressed chronic mTORC1-S6K activation and hepatosteatosis in livers of obese $Sesn2^{-/-}$ mice while it promoted insulin-induced AKT activation. Therefore, chronic downregulation of AMPK activity upon Sestrin2 deficiency results in enhanced mTORC1 activation, thereby attenuating insulin-induced AKT activity. This effect is presumably due to the phosphorylation of IRS proteins at their negative regulatory sites by the mTORC1 target S6K (Um et al., 2004). Consistent with this model, hepatocyte-specific ablation of TSC1, which causes mTORC1-S6K hyperactivation, strongly inhibited insulin-induced AKT phosphorylation and caused glucose homeostasis defects (Yecies et al., 2011). However, hepatocyte-specific ablation of AMPK did not cause spontaneous insulin resistance on its own (Foretz et al., 2010), raising the possibilities that homeostatic function of AMPK may be redundantly performed by other AMPK-related kinases or that AMPK regulation in tissues other than liver may be also important. Therefore, future studies should examine whether AMPK-related kinases are also regulated by the Sestrins and whether the function of Sestrin2 in other organs, such as adipose tissue, makes a contribution to the observed $Sesn2^{-/-}$ metabolic phenotypes. Interestingly, ectopic expression of Sestrin2 and other Sestrin family members induces AKT phosphorylation, even in cells that are not acutely stimulated with insulin. Sestrin-dependent activation of AKT is also observed in *Drosophila* and appears to be mediated via AMPK and TSC2, whose activity can potentiate activation of mTORC2, the AKT Ser473 kinase. Clearly, the ability of Sestrins to promote AMPK activation, suppress mTORC1-S6K signaling and activate AKT is not cell type specific and therefore takes place in many different tissues.

It should be noted that unlike *Sesn2*$^{-/-}$ mice, mice with hepatocyte-specific TSC1 ablation do not experience aggravated hepatosteatosis during obesity (Yecies et al., 2011). This is probably due to the different mechanisms of action of TSC1 and Sestrin2; unlike TSC1, Sestrin2 activates AMPK which can control lipid metabolism in mTORC1-independent ways (Kahn et al., 2005). For example, AMPK phosphorylates and inactivates ACC, reducing fatty acid synthesis and indirectly stimulating mitochondrial import and oxidation of fatty acids. AMPK also phosphorylates and activates ULK1/ATG1, which initiates autophagy (Egan et al., 2011). In addition, AMPK can promote mitochondrial biogenesis, which can increase β-oxidation (Canto et al., 2009). These metabolic outputs of AMPK are decreased upon Sestrin2 deficiency, and as a result *Sesn2*$^{-/-}$ livers exhibit diminished β-oxidation and aggravated hepatosteatosis during obesity. In addition, Sestrin2 deficiency resulted in the absence of LD-associated autophagosomes, which are presumably the major pathway for LD digestion and utilization in hepatocytes (Singh et al., 2009). Another contributor could be SREBP1 whose processing was modestly enhanced by Sestrin2 loss, although lipogenic gene expression and *de novo* lipogenesis in the *Sesn2*$^{-/-}$ liver were not significantly increased. Regardless of the relative contribution of these molecular conduits to hepatosteatosis in *Sesn2*$^{-/-}$ mice, it is unlikely that hepatosteatosis *per se* is responsible for the metabolic defects in these mice, as certain strains of mice can exhibit fatty liver without marked metabolic abnormalities (Farese et al., 2012). Further supporting this idea, *Sesn2*$^{-/-}$/*Sesn3*$^{-/-}$ mice exhibit hepatic insulin resistance without displaying any signs of aberrant fat accumulation in liver.

Our results indicate that Sestrin2 is the only Sestrin protein which is inducible upon hypernutrition and obesity in mouse liver. Therefore, although *Sesn2*$^{-/-}$ mice continue to express Sestrin1 and Sestrin3, they are clearly more insulin resistant and glucose intolerant than control mice when rendered obese. As a result, *Sesn2*$^{-/-}$/*Lep*$^{ob/ob}$ mice become extremely diabetic, while *Sesn2*$^{+/-}$/*Lep*$^{ob/ob}$ mice display relatively mild insulin resistance. In addition, obese *Sesn2*$^{-/-}$ mice accumulate more lipids in their livers than Con mice. These pronounced phenotypes, however, are unlikely due to unique biochemical functions of Sestrin2 that are not shared with Sestrin1 and Sestrin3. Cell culture studies indicate that all three mammalian Sestrins as well as dSestrin can potentiate AMPK activation and the defects exhibited by *Sesn2*$^{-/-}$ mice are consistent with reduced AMPK activity and subsequent increase in mTORC1 activation. Indeed, combined Sestrin 2 and 3 deficiency causes insulin resistance in non-obese mice and alters mTORC1-S6K signaling in both liver and muscle. It is also worth mentioning that ATM/p53 signaling mutations in humans and mice, which strongly reduce hepatic expression of Sestrin1–3, are associated with insulin resistance and aberrant glucose metabolism (Armata et al., 2010; Bar et al., 1978; Schneider et al., 2006). Given their induction by genotoxic stress and their ability to control glucose and lipid homeostasis, the Sestrins may represent the missing link between DNA damage and metabolism.

Experimental Procedures

Mice and Diets

Sesn2$^{-/-}$ mice (Budanov and Karin, 2008) were backcrossed to the C57BL/6 strain for at least 7 generations. *Sesn3*$^{-/-}$ mice on the C57BL/6 background were generated from ES cells obtained from EUCOMM. These cells were created by targeted gene trap approach and contain reporter-tagged insertion within intron 5 of the *Sesn3* gene with a strong splice acceptor site expressing a β-gal-Neo fusion protein that disrupts the *Sesn3* ORF. *Lep*^{ob} mice also in the C57BL/6 background were purchased from the Jackson Lab. Mice were maintained in filter-topped cages and were given free access to autoclaved regular chow diet (LFD) or high-fat diet (HFD, composed of 59% fat, 15% protein, 26% carbohydrates based

on caloric content; Bio-Serv) and water at UCSD or UM according to NIH and institutional guidelines.

Mammalian Cell Culture and Biochemical Assays

MCF7-tet OFF Sesn2F cells were described (Budanov and Karin, 2008). Immortalized *Sesn2*$^{+/+}$ and *Sesn2*$^{-/-}$ fibroblasts were generated by infecting MEF with a lentiviral vector expressing ARF1 shRNA. Immortalized *Ampka1*$^{-/-}$/*Ampka2*$^{-/-}$ fibroblasts were described (Laderoute et al., 2006), and *Tsc2*$^{+/+}$ and *Tsc2*$^{-/-}$ immortalized fibroblasts were obtained from D. Kwiatkowsky. Cell culture conditions, MCF7-tet OFF system, and infection with retroviral vectors were described (Budanov and Karin, 2008). Immunoblotting, RNA analysis, immune complex kinase assay, lipid metabolism assays, and adenoviral procedures are described in Supplemental Experimental Procedures.

Evaluation of Glucose Homeostasis

For glucose and insulin tolerance tests, mice were starved for 6 or 12 hrs as indicated. Blood was drawn from a tail nick at the indicated time points after i.p. injection of glucose (1g/kg body weight) or insulin (0.65U/kg body weight), and blood glucose was instantly measured using one-touch ultra glucose meter. Hyperinsulinemic-euglycemic clamps were performed with an infusion of 12 mU insulin/kg body weight per minute as described (Oh et al., 2010). Glucose uptake assay in primary adipocytes and serum insulin measurement were done as described (Oh et al., 2010). Glucose in urine was quantified as in Supplemental Experimental Procedures.

Histology

EM and fluorescence staining were done as described in Supplemental Experimental Procedures. Oil Red O staining of frozen liver sections (Park et al., 2010) and immunostaining of *Drosophila* imaginal discs (Lee et al., 2010) were described.

Statistical Analysis

Data are presented as means ± standard error or means ± standard deviation as indicated in legends. *P* values were calculated using Student's t-test or two-way ANOVA as indicated.

Supplementary Material

Refer to Web version on PubMed Central for supplementary material.

Acknowledgments

We thank D. Kwiatkowsky (Harvard), R. Shaw (Salk Institute), J.E. Dixon (UCSD), J.L. Guan, S. Pletcher, R.A. Miller, A. Saltiel (UM), Developmental Studies Hybridoma Bank, Cell Signaling Inc., Santa Cruz Biotech. Inc., Biomiga Inc., Stemcell Inc., Abgent Inc., for reagents and access to lab equipment. We thank M. Kim for suggestions and constructive criticism, and A. Chen, M. Lu, H. Ogata, C.R. Sanchez and K. Kim for technical assistance. Work was supported by grants and fellowships from the NIH (CA118165, CA155120, ES006376 and P42-ES010337 to M.K., DK082080 to A.B., P30-DK034933, P30-CA46592, P30-AG024824 and P30-AG013283 to J.H.L., P41-RR004050 and P30-CA23100 to M.H.E.), Ellison Medical Foundation (AG-SS-2440-10 to M.K. and AG-NS-0932-12 to J.H.L.), American Diabetes Association (7-08-MN-29 to M.K.), Human Frontier Science Program Organization (LT00653/2008-L to J.H.L.), American Association for the Study of Liver Diseases/ American Liver Foundation (to J.H.L. and E.J.P.), and Natural Sciences and Engineering Research Council of Canada (to E.J.P.). M.K. is an American Cancer Society Professor.

References

Ali SM, Sabatini DM. Structure of S6 kinase 1 determines whether raptor-mTOR or rictor-mTOR phosphorylates its hydrophobic motif site. J Biol Chem. 2005; 280:19445–19448. [PubMed: 15809305]

Angulo P. Nonalcoholic fatty liver disease. N Engl J Med. 2002; 346:1221–1231. [PubMed: 11961152]

Armata HL, Golebiowski D, Jung DY, Ko HJ, Kim JK, Sluss HK. Requirement of the ATM/p53 Tumor Suppressor Pathway for Glucose Homeostasis. Mol Cell Biol. 2010; 30:5787–5794. [PubMed: 20956556]

Bae EJ, Xu J, Oh da Y, Bandyopadhyay G, Lagakos WS, Keshwani M, Olefsky JM. Liver-specific p70 S6 kinase depletion protects against hepatic steatosis and systemic insulin resistance. J Biol Chem. 2012; 287:18769–18780. [PubMed: 22493495]

Bar RS, Levis WR, Rechler MM, Harrison LC, Siebert C, Podskalny J, Roth J, Muggeo M. Extreme insulin resistance in ataxia telangiectasia: defect in affinity of insulin receptors. N Engl J Med. 1978; 298:1164–1171. [PubMed: 651946]

Boura-Halfon S, Zick Y. Phosphorylation of IRS proteins, insulin action, and insulin resistance. Am J Physiol Endocrinol Metab. 2009; 296:E581–E591. [PubMed: 18728222]

Budanov AV, Sablina AA, Feinstein E, Koonin EV, Chumakov PM. Regeneration of peroxiredoxins by p53-regulated sestrins, homologs of bacterial AhpD. Science. 2004; 304:596–600. [PubMed: 15105503]

Budanov AV, Karin M. p53 target genes sestrin1 and sestrin2 connect genotoxic stress and mTOR signaling. Cell. 2008; 134:451–460. [PubMed: 18692468]

Budanov AV, Lee JH, Karin M. Stressin' Sestrins take an aging fight. EMBO Mol Med. 2010; 2:388–400. [PubMed: 20878915]

Calle EE, Rodriguez C, Walker-Thurmond K, Thun MJ. Overweight, obesity, and mortality from cancer in a prospectively studied cohort of U.S. adults. N Engl J Med. 2003; 348:1625–1638. [PubMed: 12711737]

Canto C, Gerhart-Hines Z, Feige JN, Lagouge M, Noriega L, Milne JC, Elliott PJ, Puigserver P, Auwerx J. AMPK regulates energy expenditure by modulating NAD+ metabolism and SIRT1 activity. Nature. 2009; 458:1056–1060. [PubMed: 19262508]

Cao J, Xu D, Wang D, Wu R, Zhang L, Zhu H, He Q, Yang B. ROS-driven Akt dephosphorylation at Ser-473 is involved in 4-HPR-mediated apoptosis in NB4 cells. Free Radic Biol Med. 2009; 47:536–547. [PubMed: 19482076]

Chan EY. mTORC1 phosphorylates the ULK1-mAtg13-FIP200 autophagy regulatory complex. Sci Signal. 2009; 2:e51.

Chen CC, Jeon SM, Bhaskar PT, Nogueira V, Sundararajan D, Tonic I, Park Y, Hay N. FoxOs inhibit mTORC1 and activate Akt by inducing the expression of Sestrin3 and Rictor. Dev Cell. 2010; 18:592–604. [PubMed: 20412774]

Egan D, Kim J, Shaw RJ, Guan KL. The autophagy initiating kinase ULK1 is regulated via opposing phosphorylation by AMPK and mTOR. Autophagy. 2011; 7:643–644. [PubMed: 21460621]

Farese, Robert V.; Zechner, R.; Newgard, Christopher B.; Walther, Tobias C. The Problem of Establishing Relationships between Hepatic Steatosis and Hepatic Insulin Resistance. Cell metabolism. 2012; 15:570–573. [PubMed: 22560209]

Foretz M, Hebrard S, Leclerc J, Zarrinpashneh E, Soty M, Mithieux G, Sakamoto K, Andreelli F, Viollet B. Metformin inhibits hepatic gluconeogenesis in mice independently of the LKB1/AMPK pathway via a decrease in hepatic energy state. J Clin Invest. 2010; 120:2355–2369. [PubMed: 20577053]

Friedel RH, Seisenberger C, Kaloff C, Wurst W. EUCOMM--the European conditional mouse mutagenesis program. Brief Funct Genomic Proteomic. 2007; 6:180–185. [PubMed: 17967808]

Haslam DW, James WP. Obesity. Lancet. 2005; 366:1197–1209. [PubMed: 16198769]

Kahn BB, Alquier T, Carling D, Hardie DG. AMP-activated protein kinase: ancient energy gauge provides clues to modern understanding of metabolism. Cell Metab. 2005; 1:15–25. [PubMed: 16054041]

Laderoute KR, Amin K, Calaoagan JM, Knapp M, Le T, Orduna J, Foretz M, Viollet B. 5'-AMP-activated protein kinase (AMPK) is induced by low-oxygen and glucose deprivation conditions found in solid-tumor microenvironments. Mol Cell Biol. 2006; 26:5336–5347. [PubMed: 16809770]

Lamming DW, Ye L, Katajisto P, Goncalves MD, Saitoh M, Stevens DM, Davis JG, Salmon AB, Richardson A, Ahima RS, et al. Rapamycin-induced insulin resistance is mediated by mTORC2 loss and uncoupled from longevity. Science. 2012; 335:1638–1643. [PubMed: 22461615]

Laplante M, Sabatini DM. An emerging role of mTOR in lipid biosynthesis. Curr Biol. 2009; 19:R1046–R1052. [PubMed: 19948145]

Lee JH, Budanov AV, Park EJ, Birse R, Kim TE, Perkins GA, Ocorr K, Ellisman MH, Bodmer R, Bier E, et al. Sestrin as a feedback inhibitor of TOR that prevents age-related pathologies. Science. 2010; 327:1223–1228. [PubMed: 20203043]

Li Y, Xu S, Mihaylova MM, Zheng B, Hou X, Jiang B, Park O, Luo Z, Lefai E, Shyy JY, et al. AMPK Phosphorylates and Inhibits SREBP Activity to Attenuate Hepatic Steatosis and Atherosclerosis in Diet-Induced Insulin-Resistant Mice. Cell Metab. 2011; 13:376–388. [PubMed: 21459323]

Maiuri MC, Malik SA, Morselli E, Kepp O, Criollo A, Mouchel PL, Carnuccio R, Kroemer G. Stimulation of autophagy by the p53 target gene Sestrin2. Cell Cycle. 2009; 8:1571–1576. [PubMed: 19377293]

Manning BD, Cantley LC. AKT/PKB signaling: navigating downstream. Cell. 2007; 129:1261–1274. [PubMed: 17604717]

Mizushima N, Komatsu M. Autophagy: renovation of cells and tissues. Cell. 2011; 147:728–741. [PubMed: 22078875]

Nogueira V, Park Y, Chen CC, Xu PZ, Chen ML, Tonic I, Unterman T, Hay N. Akt determines replicative senescence and oxidative or oncogenic premature senescence and sensitizes cells to oxidative apoptosis. Cancer Cell. 2008; 14:458–470. [PubMed: 19061837]

Oh DY, Talukdar S, Bae EJ, Imamura T, Morinaga H, Fan W, Li P, Lu WJ, Watkins SM, Olefsky JM. GPR120 is an omega-3 fatty acid receptor mediating potent anti-inflammatory and insulin-sensitizing effects. Cell. 2010; 142:687–698. [PubMed: 20813258]

Park EJ, Lee JH, Yu G, He G, Ali SR, Holzer RG, Osterreicher CH, Takahashi H, Karin M. Dietary and genetic obesity promote liver inflammation and tumorigenesis by enhancing IL-6 and TNF expression. Cell. 2010; 140:197–208. [PubMed: 20141834]

Porstmann T, Santos CR, Griffiths B, Cully M, Wu M, Leevers S, Griffiths JR, Chung YL, Schulze A. SREBP activity is regulated by mTORC1 and contributes to Akt-dependent cell growth. Cell Metab. 2008; 8:224–236. [PubMed: 18762023]

Reiter AK, Bolster DR, Crozier SJ, Kimball SR, Jefferson LS. Repression of protein synthesis and mTOR signaling in rat liver mediated by the AMPK activator aminoimidazole carboxamide ribonucleoside. Am J Physiol Endocrinol Metab. 2005; 288:E980–988. [PubMed: 15613684]

Schneider JG, Finck BN, Ren J, Standley KN, Takagi M, Maclean KH, Bernal-Mizrachi C, Muslin AJ, Kastan MB, Semenkovich CF. ATM-dependent suppression of stress signaling reduces vascular disease in metabolic syndrome. Cell Metab. 2006; 4:377–389. [PubMed: 17084711]

Singh R, Kaushik S, Wang Y, Xiang Y, Novak I, Komatsu M, Tanaka K, Cuervo AM, Czaja MJ. Autophagy regulates lipid metabolism. Nature. 2009; 458:1131–1135. [PubMed: 19339967]

Soliman GA, Acosta-Jaquez HA, Dunlop EA, Ekim B, Maj NE, Tee AR, Fingar DC. mTOR Ser-2481 autophosphorylation monitors mTORC-specific catalytic activity and clarifies rapamycin mechanism of action. J Biol Chem. 2010; 285:7866–7879. [PubMed: 20022946]

Sondergaard L. Homology between the mammalian liver and the Drosophila fat body. Trends Genet. 1993; 9:193. [PubMed: 8337758]

Um SH, Frigerio F, Watanabe M, Picard F, Joaquin M, Sticker M, Fumagalli S, Allegrini PR, Kozma SC, Auwerx J, et al. Absence of S6K1 protects against age- and diet-induced obesity while enhancing insulin sensitivity. Nature. 2004; 431:200–205. [PubMed: 15306821]

Um SH, D'Alessio D, Thomas G. Nutrient overload, insulin resistance, and ribosomal protein S6 kinase 1, S6K1. Cell Metab. 2006; 3:393–402. [PubMed: 16753575]

Yecies JL, Zhang HH, Menon S, Liu S, Yecies D, Lipovsky AI, Gorgun C, Kwiatkowski DJ, Hotamisligil GS, Lee CH, et al. Akt stimulates hepatic SREBP1c and lipogenesis through parallel

mTORC1-dependent and independent pathways. Cell Metab. 2011; 14:21–32. [PubMed: 21723501]

Zoncu R, Efeyan A, Sabatini DM. mTOR: from growth signal integration to cancer, diabetes and ageing. Nat Rev Mol Cell Biol. 2011; 12:21–35. [PubMed: 21157483]

Highlights

- Stress-inducible Sestrins have an important homeostatic function.
- Sestrin2 prevents obesity-induced insulin resistance and diabetic progression.
- Sestrin2/3-DKO mice exhibit spontaneous mTORC1 activation and insulin resistance.
- Sestrin2 potentiates AKT activation through the AMPK-mTORC1 axis.

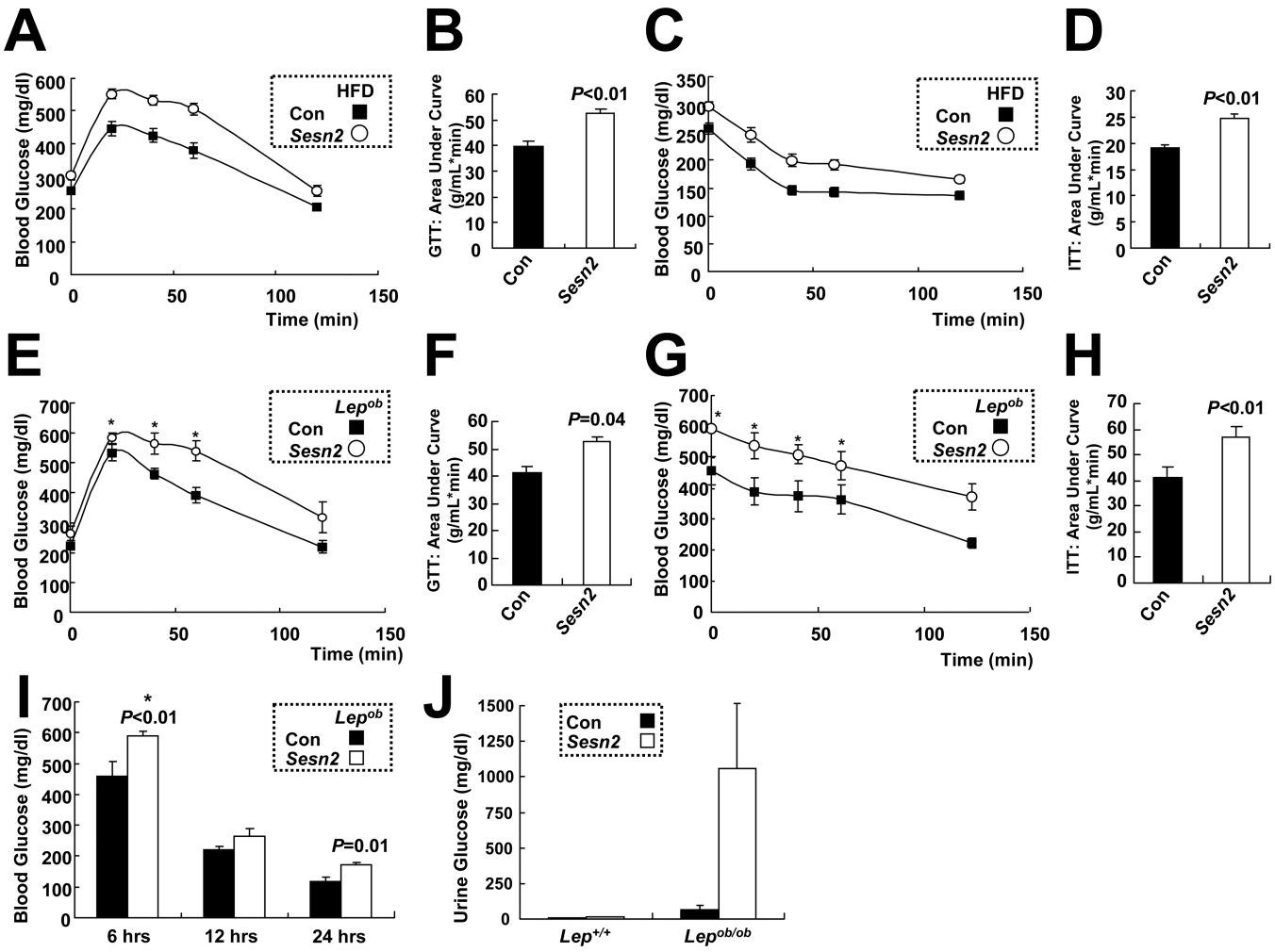

Figure 1. Sestrin2 deficiency enhances obesity-induced insulin resistance

(A–D) HFD-induced glucose intolerance and insulin resistance in WT and *Sesn2*$^{-/-}$ mice. After 6 hrs of fasting, Con (*Sesn2*$^{+/+}$ or *Sesn2*$^{+/-}$) and *Sesn2*$^{-/-}$ mice kept on HFD for 3 months were subjected to glucose tolerance test (A, GTT, n≥16) and area-under-curve analysis (B), or to insulin tolerance test (C, ITT, n≥28) and area-under-curve analysis (D). (E–H) Glucose intolerance and insulin resistance caused by leptin deficiency are aggravated by Sestrin2 deficiency. After 12 hrs (E and F) or 6 hrs (G and H) of fasting, 4 month-old *Lep*$^{ob/ob}$/*Sesn2*$^{+/-}$(Con) and *Lep*$^{ob/ob}$/*Sesn2*$^{-/-}$ (*Sesn2*) mice were subjected to GTT (E, n≥4) or to ITT (G, n≥5) and area-under-curve analyses (F, H). (I and J) Blood (I) and urine (J) glucose measurements from *Lep*$^{ob/ob}$/*Sesn2*$^{+/-}$ (Con) and *Lep*$^{ob/ob}$/*Sesn2*$^{-/-}$ (*Sesn2*) mice (n≥4) fed *ad lib* on LFD (J) or after the indicated fasting periods (I). Stars (*) denote that the data contain measurements exceeding the detection limit of the glucose meter (600 mg/dl). Thus, the star-marked data may be higher than the plotted values. Data are presented as means ± standard error. *P* values were calculated using Student's t-test.

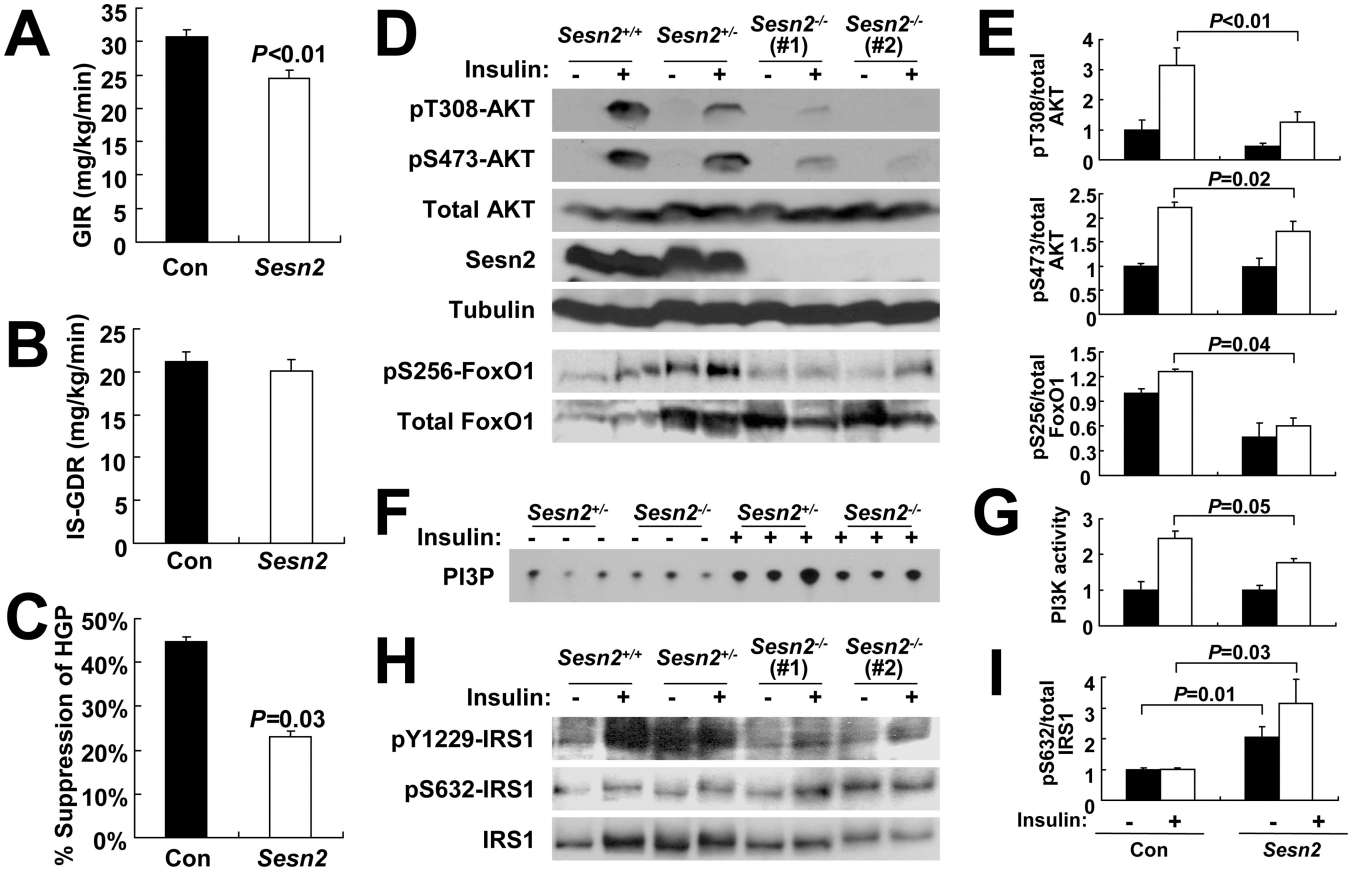

Figure 2. *Sesn2*$^{-/-}$ mice kept on HFD exhibit hepatic insulin resistance

(A–C) Glucose infusion rates (A, GIR), insulin-stimulated glucose disposal rates (B, IS-GDR), and suppression of hepatic glucose production (C, HGP) in Con and *Sesn2*$^{-/-}$ mice kept on HFD for 4 months during hyperinsulinemic-euglycemic clamp (n≥8). (D–I) Livers were collected from Con (*Sesn2*$^{+/+}$ or *Sesn2*$^{+/-}$) and *Sesn2*$^{-/-}$ mice kept on HFD for 4 months, after 6 hrs of fasting, before (−) or 10 min after (+) insulin injection (0.8U/kg body weight). (D and E) Phosphorylation of AKT at Thr308 and Ser473, and FoxO1 at Ser256, was analyzed by immunoblotting (D). Ratios of phosphorylated to total AKT (n≥8) or FoxO1 (n=5) were quantified by densitometry, and are presented as bar graphs (E). (F and G) Activity of PI3K was measured, and lipid phosphorylation was visualized by thin layer chromatography-autoradiography (PI3P, F) and quantified by densitometry (G, n=3). (H and I) Phosphorylation of IRS-1 at Tyr1229 and Ser632 was analyzed by immunoblotting (H) and the ratio of phosphorylated to total IRS-1 is presented as a bar graph (I, n=5). Data are presented as means ± standard error. *P* values were calculated using Student's t-test.

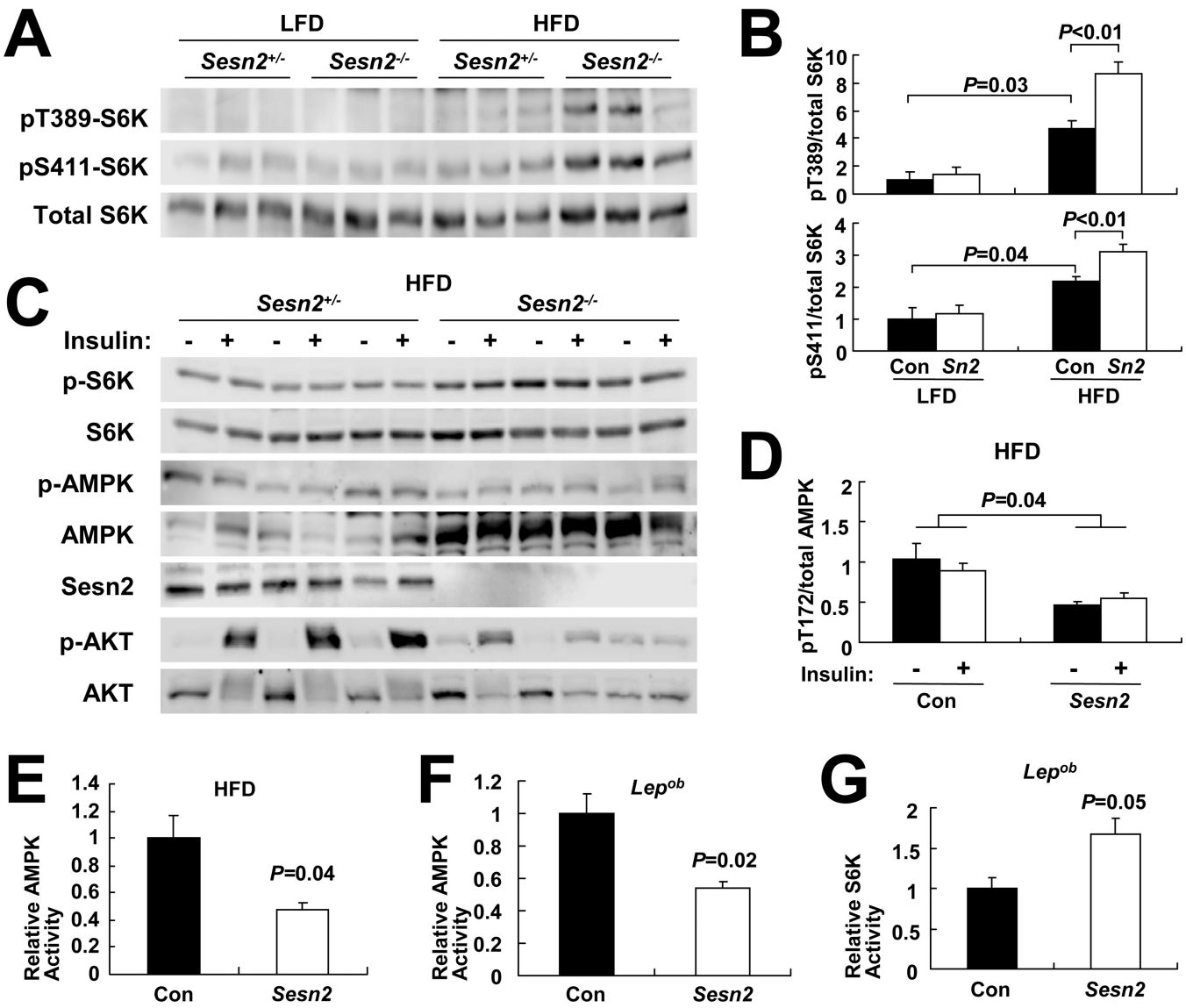

Figure 3. Sestrin2 regulates AMPK-mTORC1 signaling in liver

(A and B) Livers from 6 months-old mice of the indicated genotypes kept on LFD or HFD for 4 months were analyzed by immunoblotting for mTORC1-dependent S6K phosphorylation at Thr389 and Ser411 (A). Ratio of phosphorylated to total S6K was quantified by densitometry and presented as bar graphs (B, n≥3). (C and D) Livers were collected from *Sesn2*$^{+/-}$ and *Sesn2*$^{-/-}$mice kept on HFD, after 6 hrs of fasting, before (−) or 10 min after (+) insulin injection (0.8 U/kg body weight), and analyzed for protein phosphorylation and expression with indicated antibodies (C). Ratio of phosphorylated to total AMPK was presented as a bar graph (D, n=3). (E–G) AMPK (E and F) and S6K (G) activities in livers of HFD-fed Con and *Sesn2*$^{-/-}$ mice (E) or *Lep*$^{ob/ob}$/*Sesn2*$^{+/-}$ and *Lep*$^{ob/ob}$/*Sesn2*$^{-/-}$ mice (F and G) were measured by kinase assays (n=3). Levels of immunoprecipitated kinases and corresponding kinase activities are presented in Figure S3. Data are presented as means ± standard error. *P* values were calculated using Student's t-test or two-way ANOVA.

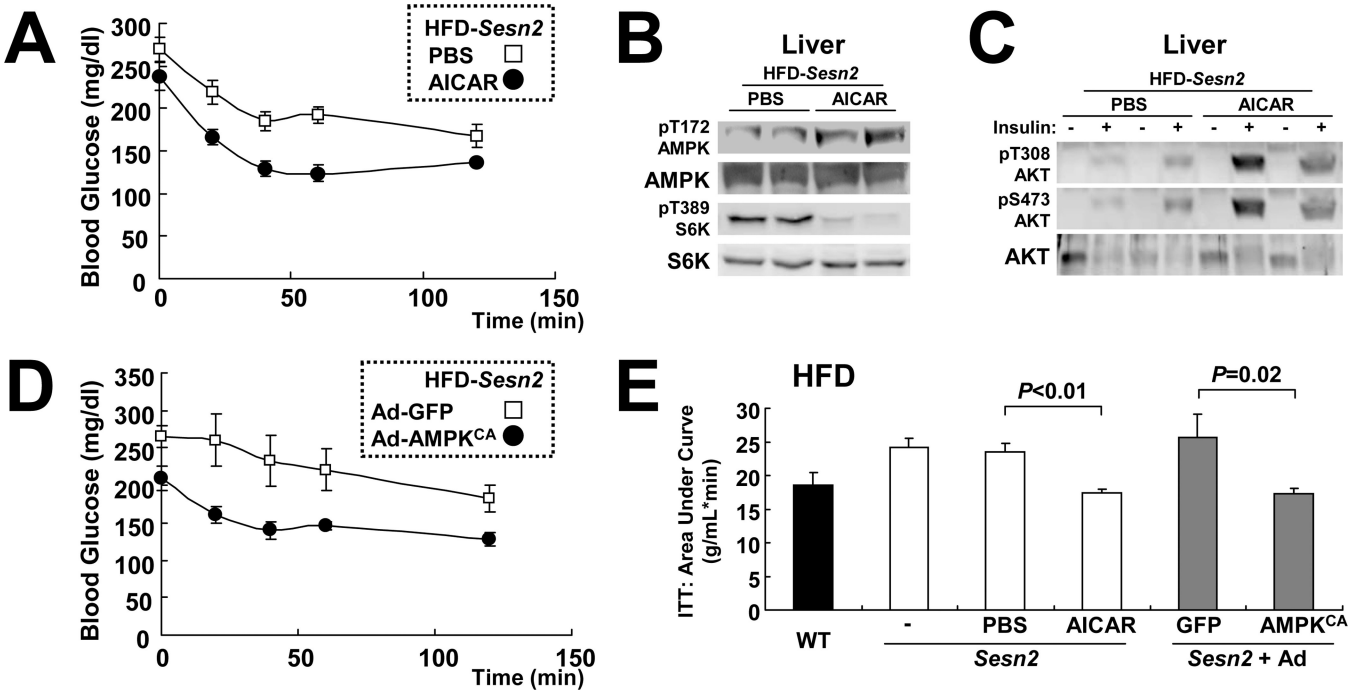

Figure 4. Reactivation of hepatic AMPK restores insulin resistance of HFD-fed *Sesn2*$^{-/-}$ mice

(A) *Sesn2*$^{-/-}$ mice kept on HFD for 3 months were subjected to daily i.p. injection of 250 mg/kg body weight AICAR or vehicle (PBS) for 5 days. After 6 hrs of fasting, the mice were subjected to ITT (n=6). (B and C) After 10 days of AICAR or vehicle (PBS) injection, livers from the mice described above were collected after 6 hrs of fasting, before (B and (−) in C) or 10 min after ((+) in C) insulin injection (0.8 U/kg body weight). The livers were analyzed for protein phosphorylation and expression with the indicated antibodies. (D) *Sesn2*$^{-/-}$ mice kept on HFD for 3 months were infected with adenoviruses expressing GFP (Ad-GFP) or constitutively active AMPK (Ad-AMPK^{CA}). After 6 hrs of fasting, ITT (n=6) was performed at 24 hrs after infection. (E) Area-under-curve analysis of ITT data. Values from untreated *Sesn2*$^{+/+}$ (WT) and *Sesn2*$^{-/-}$ (−) mice of the same HFD cohorts were provided as reference (n≥6). Data are presented as means ± standard error. *P* values were calculated using Student's t-test.

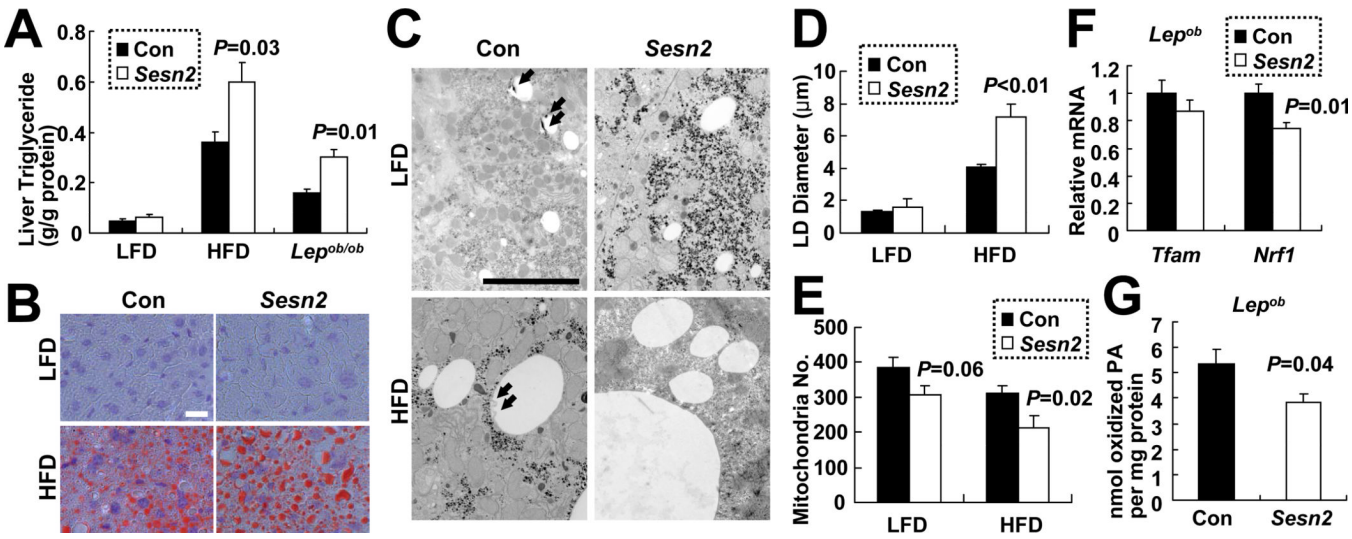

Figure 5. Sestrin2 attenuates hepatosteatosis during obesity

(A) Elevated triglycerides in obese *Sesn2*$^{-/-}$ livers. Liver triglycerides in livers of Con (*Sesn2*$^{+/+}$and *Sesn2*$^{+/-}$) and *Sesn2*$^{-/-}$ mice kept on LFD or HFD, or *Lep*$^{ob/ob}$/*Sesn2*$^{+/-}$ or *Lep*$^{ob/ob}$/*Sesn2*$^{-/-}$ mice (n≥4). (B–D) Increased LD size in obese *Sesn2*$^{-/-}$ livers. (B and C) Liver LDs were visualized using Oil Red O staining (B) and EM (C) in Con and *Sesn2*$^{-/-}$ mice kept on LFD or HFD. Putative autophagosomes associated with LDs in Con livers are indicated with arrows. Scale bars, 20 μm (white), 5 μm (black). (D) Quantification of maximum LD diameters from EM images (21.4 × 31.9 μm, n≥8). (E and F) Reduced expression of mitochondrial biogenesis marker genes in obese *Sesn2*$^{-/-}$ livers. (E) Quantification of mitochondria number per field from EM images. (F) Relative *Tfam* and *Nrf1* mRNA amounts in livers of indicated mice (n≥7). (G) β-oxidation of C^{14}-labeled palmitic acid (PA) was measured in liver homogenates of *Lep*$^{ob/ob}$/*Sesn2*$^{+/-}$ (Con) and *Lep*$^{ob/ob}$/*Sesn2*$^{-/-}$ (*Sesn2*) mice (n≥5). Data are presented as means ± standard error. *P* values were calculated using Student's t-test.

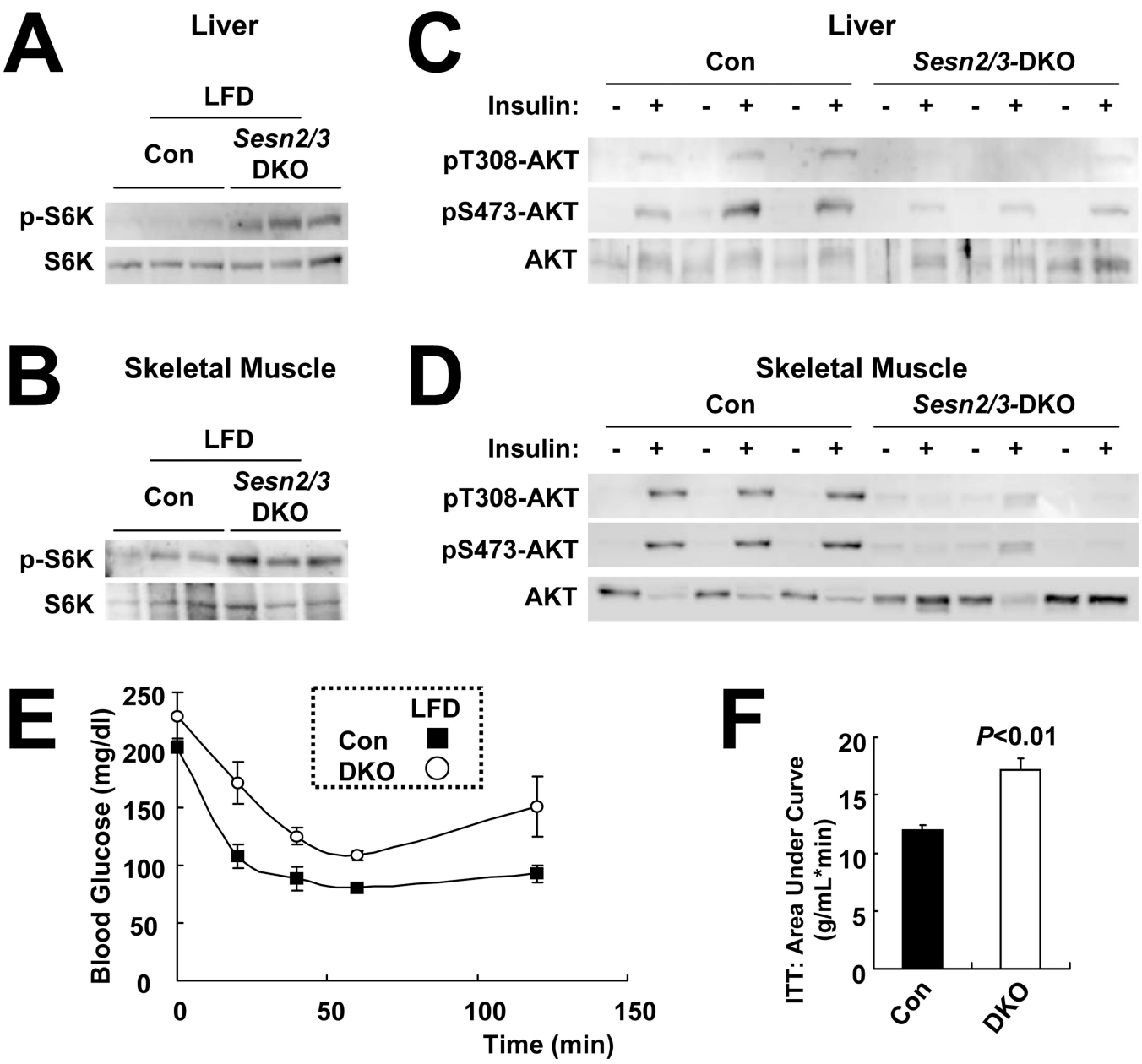

Figure 6. Ablation of Sestrin2 and 3 causes mTORC1 upregulation and spontaneous insulin resistance

(A and B) *Sesn2*$^{-/-}$/*Sesn3*$^{-/-}$ DKO mice exhibit elevated mTORC1-dependent S6K phosphorylation. Livers and skeletal muscles from three 4 month-old Con (*Sesn2*$^{+/-}$) and DKO mice kept on LFD were analyzed by immunoblotting for S6K phosphorylation on Thr389. (C and D) Livers and skeletal muscles were collected from Con and DKO mice, after 6 hrs of fasting, before (−) or 10 min after (+) insulin injection (0.8 U/kg body weight), homogenized and analyzed by immunoblotting with the indicated antibodies. (E and F) After 6 hrs of fasting, 4 month-old Con and DKO mice kept on LFD were subjected to ITT (E, n=3) and area-under-curve analysis (F). Data are presented as means ± standard error. *P* values were calculated using Student's t-test.

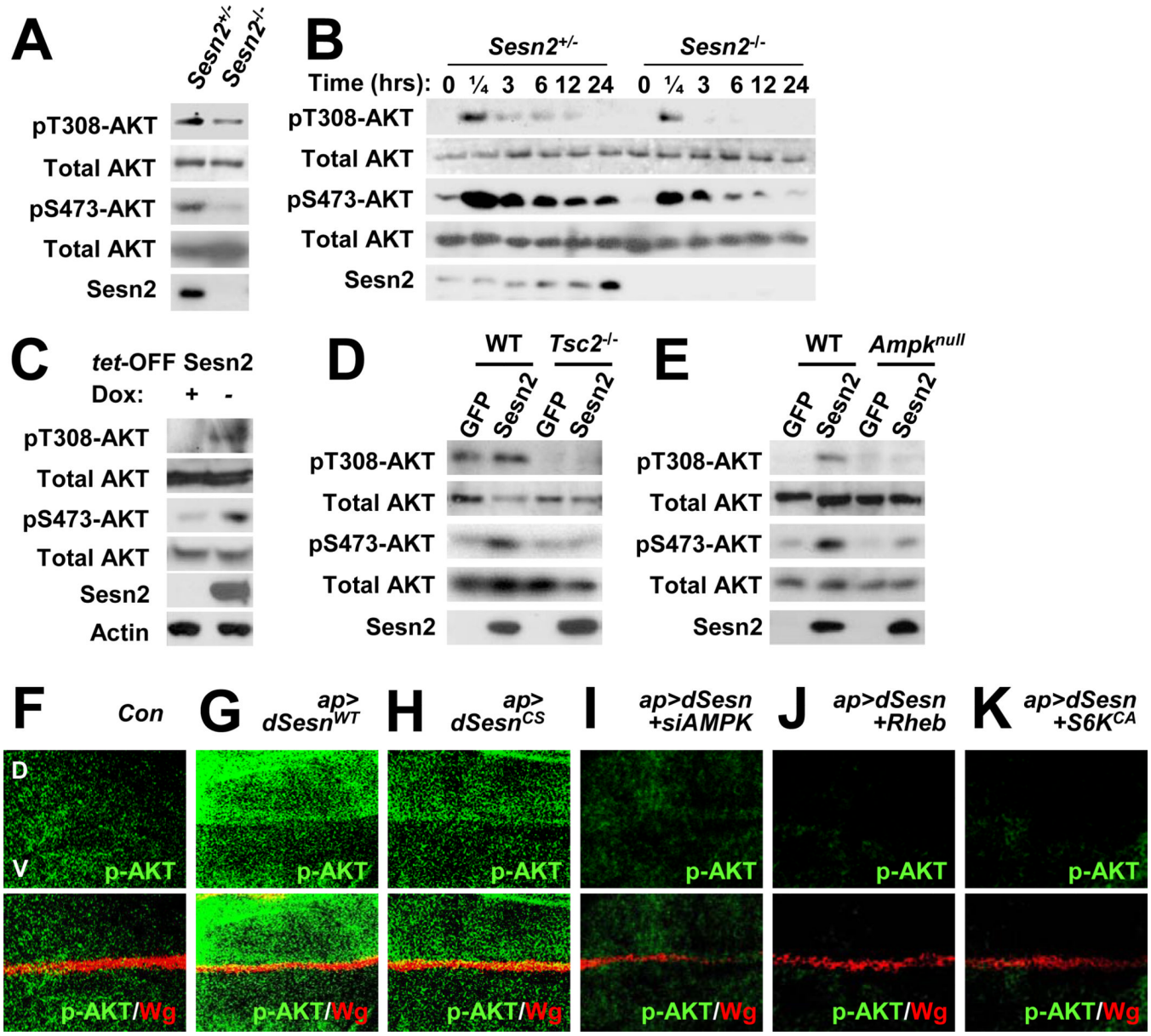

Figure 7. Sestrin2 potentiates AKT signaling through the AMPK-TSC2 axis

(A) Reduced AKT phosphorylation in *Sesn2*$^{-/-}$ MEFs. Steady state AKT phosphorylation at Thr308 and Ser473 in MEFs grown in the presence of 10% FCS was examined by immunoblotting. (B) Reduced insulin-stimulated AKT phosphorylation in *Sesn2*$^{-/-}$ MEFs. After 24 hrs of serum starvation, MEFs were collected at the indicated times after insulin treatment and analyzed for AKT phosphorylation. (C) Sestrin2 stimulates AKT signaling. Flag-tagged Sestrin2 was induced in MCF7-tet OFF Sesn2F cells by doxycycline (Dox) removal (−). Control cultures were left with Dox (+). Cell lysates prepared after 24 hrs were analyzed for expression and phosphorylation of the indicated proteins. (D and E) Sestrin2 activation of AKT is TSC2 and AMPK dependent. WT, *Tsc2*$^{-/-}$ or *Ampkα1*$^{-/-}$/*Ampkα2*$^{-/-}$ (*Ampk*^{null}) MEFs were infected with lentiviral vectors encoding GFP or Flag-tagged Sestrin2 (Sesn2). Protein phosphorylation and expression were examined at 48 hrs post infection by immunoblotting. (F–K) Activation of AKT by dSestrin in *Drosophila* wing imaginal discs. Larval wing discs of the indicated strains were stained to visualize AKT

phosphorylation at Ser505 (p-AKT, equivalent to Ser473 in mice). The dorsal side points upwards. Dorsoventral boundary (D/V in F) was visualized by staining with an antibody to the wingless protein (Wg). Indicated transgenic elements were overexpressed only in the dorsal compartment as described (Lee et al., 2010).